Phase-matching measurements and Sellmeier equations over the complete transparency range of $KTiOAsO_4$, $RbTiOAsO_4$, and $CsTiOAsO_4$

Jean-Philippe Fève, Benoît Boulanger, Olivier Pacaud, Isabelle Rousseau, Bertrand Ménaert, and Gérard Marnier

Laboratoire de Physique de l'Université de Bourgogne, Unité Mixte de Recherche, Central National de la Recherche Scientifique 5027, 9 avenue A. Savary, B.P. 47870, 21078 Dijon Cedex, France

Philippe Villeval and Christophe Bonnin

Cristal Laser S.A., B.P. 44, 54230 Chaligny, France

G. M. Loiacono and D. N. Loiacono

Crystal Associates, Inc., 31 Farinella Drive, East Hanover, New Jersey 07936

Received September 13, 1999

The sphere method is used for the direct measurement of sum- and difference-frequency generation phase matched in the principal planes of $KTiOAsO_4$, $RbTiOAsO_4$, and $CsTiOAsO_4$, including the tuning curves of 1.064-μm-pumped OPO's emitting between 3 and 5 μm. The nonlinear least-squares fitting of our experimental data leads to refined dispersion equations of the principal refractive indices; the resulting dual-oscillator form equations are valid over the complete transparency range of the three studied materials. © 2000 Optical Society of America [S0740-3224(00)01505-8]

OCIS codes: 190.2620, 190.4400, 160.4330, 160.4760, 160.1190.

1. INTRODUCTION

The arsenate isomorphs of $KTiOPO_4$ are extensively studied for optical frequency conversion in the near- and mid-infrared, with special attention paid to their potential use in optical parametric oscillators (OPO's), emitting in the atmospheric transparency range 3–5 μm. Experiments have mainly been realized, with a femtosecond Ti:sapphire laser as the pump, for $KTiOAsO_4$ (Ref. 1) (KTA), $RbTiOAsO_4$ (Refs. 2 and 3) (RTA), and $CsTiOAsO_4$ (Ref. 4) (CTA). These studies show the complementarity of the three arsenate isomorphs for OPO emission between 1 and 3 μm. Sum- and difference-frequency generations involving longer wavelengths (as long as 4.2 μm) are reported in KTA[5] and RTA.[6] The published dispersion equations of the refractive indices of these compounds are based on the above-mentioned phase-matching data, and on direct prism measurements of the refractive indices as large as 3.5 μm in the case of KTA[7] and RTA.[6]

Nevertheless, these Sellmeier coefficients are not reliable over the complete transparency range of these materials, especially for KTA and CTA. This issue is of prime interest for the practical realization of efficient OPO's: The exact knowledge of the phase-matching directions ensures the cutting of the nonlinear crystal with a precision better than 1°, and so the propagation under normal incidence of the waves in the OPO is ensured; for the recent quasi-phase-matched devices based on periodically poled crystals, the coherence length of the interaction is not accurately predicted by the published Sellmeier equations, even in the case of RTA.[8]

This paper presents the measured phase-matching directions of the three arsenate isomorphs over their complete transparency range, between 0.4 and 5.3 μm; we then deduce enhanced dispersion equations of their refractive indices.

2. EXPERIMENTAL RESULTS

The measurement method based on the sphere experiment is presented elsewhere[9,10] and not detailed in this paper. The three studied crystals have been synthetized by flux methods: KTA was grown in our laboratory with a halide flux,[11] RTA was made from a halide flux at Cristal Laser,[11] and CTA was realized at Crystal Associates by use of a $Cs_5As_3O_{10}$ solvent.[12] The polished spheres' diameters are 2.45, 6, and 4 mm for KTA, RTA, and CTA, respectively.

The phase-matching properties are studied in the principal planes $x-z$ and $y-z$ of the crystals; the orthonormal (x, y, z) optical frame is identical to the crystallographic axes (a, b, c) with c the binary axis of the 2-mm orthorhombic crystal class. The directions of propagation are referred to by their spherical coordinates θ and ϕ: $\phi = 0°$ in the $x-z$ plane and $\phi = 90°$ in the $y-z$ plane. The phase-matching directions in these planes involve simple combinations of the principal refractive indices as

detailed in Section 3; furthermore, for a given interaction in this crystal class, the most efficient conversion is obtained in the $x-z$ plane in which the phase-matched conversion efficiency is governed by the χ_{24} nonlinear coefficient.

We study sum- and difference-frequency generations (SFG and DFG, respectively). A tunable beam emitted by an OPO (λ_i between 0.72 and 2.2 μm) is mixed with a beam at a fixed wavelength ($\lambda_p = 1.064\ \mu$m) delivered from the pump laser of the OPO. The interaction of these waves directly into the nonlinear spherical crystal generates wavelengths at $\lambda_g = (\lambda_p^{-1} + \lambda_i^{-1})^{-1}$ for SFG and $\lambda_g = (\lambda_p^{-1} - \lambda_i^{-1})^{-1}$ for DFG. We also consider the particular case of second-harmonic generation (SHG) $\lambda_g = \lambda_f/2$; in this case, the fundamental beam at λ_f is the tunable one coming out of the OPO.

For each interaction, two configurations of polarizations of the three interacting waves allow phase matching in the principal planes with a nonzero effective nonlinear coefficient.[13] The experimental results are summarized in Figs. 1–4 with the corresponding configurations of polarizations: An ordinary wave is polarized along the y axis in the $x-z$ plane and along the x axis in the $y-z$ plane; the extraordinary wave is polarized in the $x-z$ or $y-z$ plane.

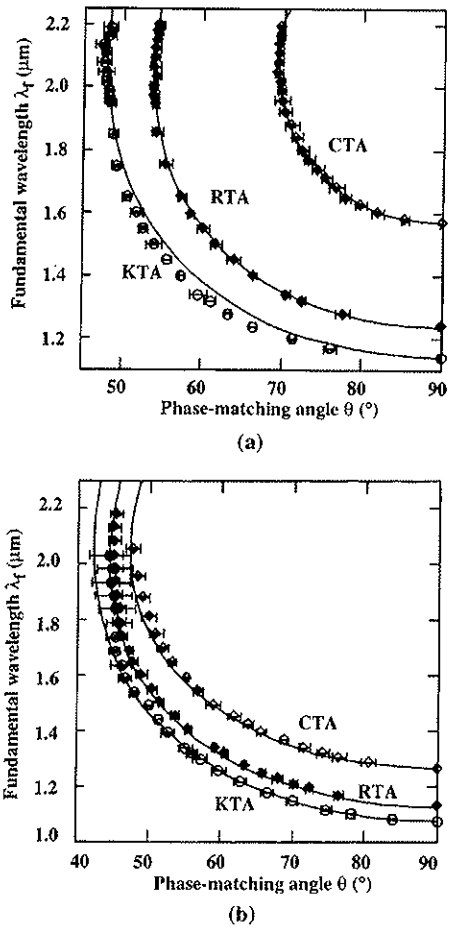

Fig. 1. Measured and calculated phase-matching curves in (a) the $x-z$ plane and (b) the $y-z$ plane of KTA, RTA, and CTA for type II SHG: $\lambda_f^o + \lambda_f^o \rightarrow \lambda_g^o$. λ_f is generated from the tunable OPO.

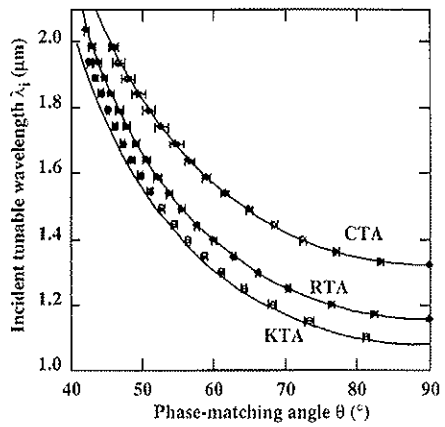

Fig. 2. Measured and calculated phase-matching curves in the $y-z$ plane of KTA, RTA, and CTA for type II SFG: $\lambda_p^e + \lambda_i^o \rightarrow \lambda_g^o$. λ_i is generated from the tunable OPO; $\lambda_p = 1.064\ \mu$m.

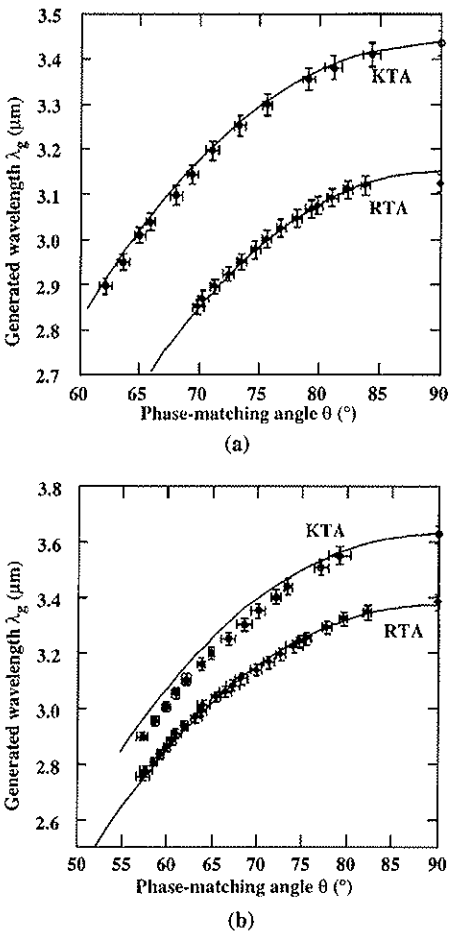

Fig. 3. Measured and calculated phase-matching curves in (a) the $x-z$ plane and (b) the $y-z$ plane of KTA and RTA for type I DFG: $\lambda_p^o - \lambda_i^o \rightarrow \lambda_g^e$. λ_i is generated from the tunable OPO; $\lambda_p = 1.064\ \mu$m.

We use a germanium filter to cut the residual nonconverted beams at λ_i and 1.064 μm for the DFG measurements; then these experiments are limited to $\lambda_i \leqslant 1.7\ \mu$m (thus $\lambda_g \geqslant 2.8\ \mu$m) because of the germanium transparency. Thus Figs. 3(a) and 3(b) are restricted to RTA and KTA, because type I DFG in CTA is phase matched for $\lambda_g \leqslant 2.6\ \mu$m. For the three compounds, the study of type II SFG in one principal plane is sufficient to complete the data of type III DFG, which corresponds to the same phase-matching relation, according to the convention in Ref. 13. Type III SFG, which corresponds to the same phase-matching relation as type I DFG, is not considered here: No phase matching exists in the case of CTA for the wavelengths delivered by the experimental setup; the phase matching is possible for KTA and RTA but for a very small spectral range and with corresponding directions located in a restricted part of the $x-y$ and $y-z$ planes.

The experimental results described in this section are discussed in Section 4 together with the fitted dispersion equations.

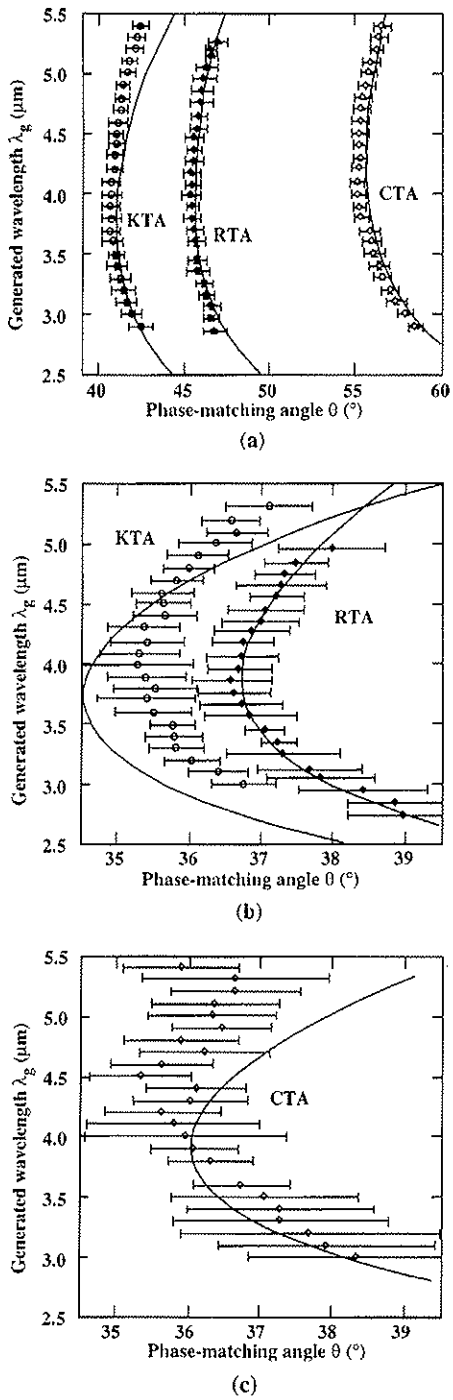

Fig. 4. Experimental phase-matching curves in (a) the $x-z$ plane of KTA, RTA, and CTA, (b) the $y-z$ plane of KTA and RTA, and (c) the $y-z$ plane of CTA for type III DFG: $\lambda_p^o - \lambda_i^e \rightarrow \lambda_g^o$. λ_i is generated from the tunable OPO; $\lambda_p = 1.064\ \mu$m.

3. SELLMEIER EQUATIONS

As proposed by Roberts,[14] accurate phase-matching data lead to refined dispersion equations of the refractive indices in the case of nonlinear optical crystals. For biaxial crystals, useful data are also provided by the dispersion in wavelength of the direction of the optical axes lying in the $x-z$ plane: This axis corresponds to the intersection of two sheets of index surfaces as any phase-matching direction; it is easily measured with the sphere method.[15] These additional data are measured in the visible spectrum to complete the phase-matching experiments: This is important because reliable dispersion equations require initial data well spread over the entire transparency range of the material.

The different phase-matching angles θ_{PM} are linked to the principal refractive indices by simple analytical relations, because the interactions we consider involve only one double-refraction angle,

$$\cos^2\theta_{PM} = \left\{\left[\frac{\lambda_a}{\lambda_c}n_a(\lambda_c) - \frac{\lambda_a}{\lambda_b}n_a(\lambda_b)\right]^{-2} - n_z^{-2}(\lambda_a)\right\} \Big/ [n_\beta^{-2}(\lambda_a) - n_z^{-2}(\lambda_a)], \quad (1)$$

where n_i corresponds to the principal refractive indices ($i = \alpha, \beta, z$) at the considered wavelength λ_a, λ_b, λ_c with

$\lambda_c = \lambda_p$, $\lambda_a = \lambda_g$, $\lambda_b = \lambda_i$ for type I DFG,

$\lambda_c = \lambda_p$, $\lambda_a = \lambda_i$, $\lambda_b = \lambda_g$ for type III DFG,

$\lambda_c = \lambda_g$, $\lambda_a = \lambda_i$, $\lambda_b = \lambda_p$ for type II SFG,

$\lambda_i = \lambda_g$ for type II SHG,

where λ_p, λ_i, λ_g are defined above; $(n_\alpha, n_\beta) = (n_x, n_y)$ in the $y-z$ plane and (n_y, n_x) in the $x-z$ plane. For the optical axes θ_{OA}, we have

$$\cos^2\theta_{OA}(\lambda) = 1 - \frac{n_y^{-2}(\lambda) - n_x^{-2}(\lambda)}{n_z^{-2}(\lambda) - n_x^{-2}(\lambda)}. \quad (2)$$

The nonlinear least-squares fitting has to be made simultaneously for all the experimental data. Thus our experimental results are stored in a single spreadsheet, with one column for wavelengths and one column for $\cos^2\theta$.

Our data are not directly weighted but rather associated with their experimental accuracies in a third column of the spreadsheet: $\Delta(\cos^2\theta) = 2\cos\theta\sin\theta\Delta\theta$ [with $\Delta\theta$ typically ranging between 0.3° and 0.8° (Ref. 10)].

The nonlinear least-squares fitting is made with the commercial software Profit 5.0, which uses various algorithms. Our calculation begins with a simplex-iteration method that is less sensitive to arbitrary initial parameters (this is checked by use of very different sets of initial parameters). This first step allows us to determine the most appropriate form of the dispersion equations: Various computations are realized with the principal refractive indices described by single oscillator equations and dual oscillator equations, with additional infrared correction.[14] For the three arsenate isomorphs KTA, RTA, and CTA, the results are unambiguous: Good and fast convergence is obtained only with a dual oscillator form,

$$n_i^2 = A_i + \frac{B_i\lambda^{p_i}}{\lambda^{p_i} - C_i} + \frac{D_i\lambda^{q_i}}{\lambda^{q_i} - E_i}, \qquad (3)$$

where $i = x, y, z$.

The second step of the fitting uses the Levenberg–Marquardt algorithm to ensure better convergence, and the exponents p_i and q_i considered as fixed parameters $p_i = q_i = 2$ during these two steps are fitted in a final third round.

Starting from our experimental data, we precisely determine the dispersion of the refractive indices, but we cannot find their absolute values. This problem is solved by adding in our data set the value of one refractive index deduced from published prism measurements, i.e., $n_z(1.064\,\mu\text{m}) = 1.8679$ for KTA,[7] $n_z(1.064\,\mu\text{m}) = 1.8808$ for RTA,[6] and $n_z(1.064\,\mu\text{m}) = 1.9204$ for CTA.[16]

The coefficients of the obtained Sellmeier equations are summarized in Table 1 with the values of chi square (sum of the squares of the deviations) at the end of the fitting procedure. The following points should be mentioned:

- Figure 5 shows the wavelength ranges covered by the experimental data, according to relations (1) and (2). For the refractive indices n_x and n_y, the complete transparency range of the crystals is well described, so that the corresponding Sellmeier equations are valid between 0.4 and 5.3 μm.

In contrast, infrared data are not available for n_z (for RTA, we did not consider the published quasi-phase-matching data,[8] because the corresponding spectral linewidth is very important between 3 and 5 μm). Thus the validity of the n_z coefficients is restricted to wavelengths below 3.6 μm for RTA and KTA and below 2.1 μm for CTA. Thus, for example, our dispersion equation for n_z does not accurately describe quasi-phase-matching properties at long wavelengths: For a 0.909-μm-pumped RTA–OPO emitting at 4.98 μm, the calculated coherence length is 13.7 μm instead of the measured 15 μm.[8]

- The corresponding calculated phase-matching curves are shown on Figs. 1 to 4. They are in better agreement with the experimental data whenever compared with the calculations made with the dispersion equations of the literature.

This is illustrated with the example of type III DFG in the x–z plane of CTA shown in Fig. 6: The average difference between experiments and calculations is nil with the equations of Table 1, whereas it is ~6° with the Sell-

Table 1. Sellmeier Coefficients for KTA, RTA, and CTA, Corresponding to the Dispersion Eq. (3) with λ in μm[a]

	Parameters	$KTiOAsO_4$	$RbTiOAsO_4$	$CsTiOAsO_4$
n_x	A_x	2.1495	2.3162	2.0408
	B_x	1.0203	0.9187	1.2924
	C_x	0.042378	0.047651	0.047575
	D_x	0.5531	9.6192	1.9304
	E_x	72.3045	841.2982	156.5049
	p_x	1.9951	1.9965	2.0008
	q_x	1.9567	2.0020	1.9874
	λ_x^{UV} (μm)	0.205	0.217	0.218
	λ_x^{IR} (μm)	8.92	28.91	12.71
n_y	A_y	2.1308	2.4674	2.4330
	B_y	1.0564	0.7906	0.9591
	C_y	0.042523	0.057959	0.068339
	D_y	0.6927	2.1021	4.2292
	E_y	54.8505	211.900	305.9224
	p_y	2.0017	1.9936	1.9853
	q_y	1.7261	1.9764	1.9338
	λ_y^{UV} (μm)	0.206	0.240	0.259
	λ_y^{IR} (μm)	10.18	15.03	19.29
n_z	A_z	2.1931	2.5902	2.5723
	B_z	1.2382	0.8983	1.0532
	C_z	0.059171	0.072667	0.080077
	D_z	0.5088	0.7528	0.6178
	E_z	53.2898	68.6252	40.7806
	p_z	1.8920	1.9851	2.0297
	q_z	2.0000	2.0099	1.9934
	λ_z^{UV} (μm)	0.224	0.267	0.288
	λ_z^{IR} (μm)	7.30	8.20	6.43
Chi-square		742.26	27.84	102.24
	N	163	175	126

[a] The resonance wavelengths are $\lambda_i^{UV} = p_i\sqrt{C_i}$ and $\lambda_i^{IR} = q_i\sqrt{E_i}$. These equations are valid between 0.4 and 5.3 μm for n_x and n_y in the three isomorphs, between 0.4 and 3.6 μm for n_z in KTA and RTA, and between 0.4 and 2.1 μm for n_z in CTA. N, number of independent measured data.

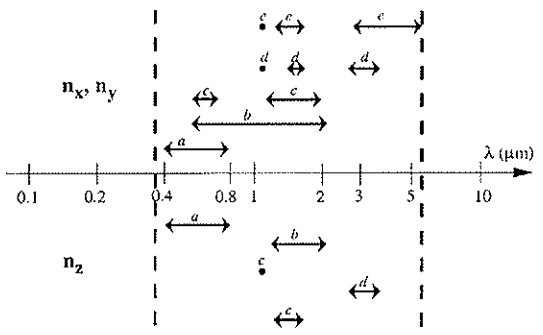

Fig. 5. Wavelength ranges covered by the experimental data for the refractive indices $n_{x,y}$ and n_z. The vertical dashed lines indicate the transparency range of the crystals. The different types of data are denoted by *a*, optical axes; *b*, type II SHG; *c*, type II SFG; *d*, type I DFG; and *e*, type III DFG.

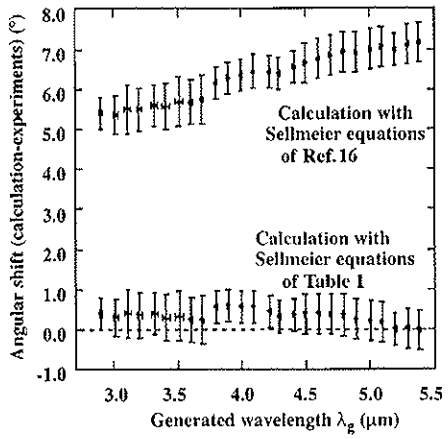

Fig. 6. Comparison between measured phase-matching directions and the calculations for two different dispersion equations in the case of type III DFG in the x–z plane of CTA.

meier coefficients of Ref. 16; this corresponds to an external angular shift ~11°. If we assume that the error is due only to the refractive index at the longest wavelength λ_g, the corresponding discrepancy is $\Delta n_y = 0.010$ at $\lambda_g = 3\ \mu$m and $\Delta n_y = 0.027$ at $\lambda_g = 5\ \mu$m.

- A similar enhancement is obtained for the other interaction types in CTA and in KTA. Nevertheless, for DFG involving long wavelengths in KTA, we observe a nonzero discrepancy between experiments and calculations, of the order of 1°. This is coherent with the residual chi square, which is much higher in the case of KTA, as shown in Table 1. For RTA, the enhancement is lower because the dispersion equations of Ref. 6 are accurate to as much as 4 μm.
- The fitted exponents p_i and q_i given in Table 1 remain very close to 2, which indicates that Eq. (3) is adequate for these materials and that no additional oscillator is required.[14]
- The dispersion equations of KTA exhibit an uniaxial behavior ($n_x = n_y$) at 2.54 μm. All previously published Sellmeier equations for this compound lead to such a result, even if the corresponding wavelength is different, from 2.4 (Ref. 16) to 4.1 (Ref. 5) or 5 μm.[7]
- The resonance wavelength of the ultraviolet oscillators, $\lambda_i^{UV} = {}^{p_i}\sqrt{C_i}$, given in Table 1 are such as $\lambda_x^{UV} < \lambda_y^{UV} < \lambda_z^{UV}$ for the three compounds. This anisotropy is also observed in experimental transmission spectra of KTA, RTA, and CTA with polarized light: The cutoff wavelength are found in the same order, $\lambda_x^{UV} < \lambda_y^{UV} < \lambda_z^{UV}$, between 340 and 370 nm. The infrared resonance wavelengths of Table 1, $\lambda_i^{IR} = {}^{q_i}\sqrt{E_i}$, are located above 9 μm, except for n_z. This should be compared with the infrared reflectivity spectra of KTP[17] and to the absorption spectra measured in KTP and KTA[18]: These data show that the shortest resonance wavelength is ~9μm for the phosphate compounds and ~11 μm for the arsenate isomorphs.

Thus, starting from arbitrary initial conditions, our refined Sellmeier coefficients are coherent with the basic solid-state physics data relative to the studied materials.

4. DISCUSSION AND CONCLUSION

The results of Figs. 4(a), 4(b), and 4(c) are of prime interest for the realization of OPO's emitting in the 3–5 μm range: They confirm that the arsenate isomorphs are the preferred materials for such frequency conversion. Type III DFG generates a tunable wavelength over the 3–5 μm range for a very small associated angular deviation, between 2° and 3°. Thus the nonlinear crystal should be cut for a propagation along the average angle of that angular domain: The OPO will work with very small incidence angles and emit high-quality beams.

As shown in Figs. 3(a) and 3(b), type I DFG also offers interesting phase-matching properties, especially for eye-safe emission: The generated signal wavelength is 1.54 μm along the x axis of KTA and 1.55 μm along the y axis of RTA, both for 1.064-μm-pumped OPO. These angular noncritical phase matchings allow very high conversion efficiencies, as recently demonstrated with KTA pumped with a picosecond laser.[19] Furthermore, in contrast to the classical KTP devices, the associated idler beam ~3.4 μm is not absorbed by the arsenate crystals, leading to an enhanced stability. The corresponding nonlinear effective coefficient is larger along the x axis of KTA whenever compared with the y axis of RTA (5.29 pm/V and 2.75 pm/V, respectively[9]). Nevertheless, RTA will often be preferred to KTA and CTA because of easier crystal growth. An interesting noncritical phase-matching situation occurs for type II SFG along the y axis of CTA: It corresponds to the two laser lines of the Nd:YAG laser, 1.064 and 1.32 μm.

The knowledge of the dispersion equations is also very interesting for the choice of the different materials in the case of tight focusing experiments, in which spatial walk-off attenuates the conversion efficiency. This is illustrated with the example of type I DFG shown on Fig. 7. We calculate the plane-wave conversion efficiency of the DFG interaction as a function of the generated wavelength λ_g for a given crystal length ($L = 10$ mm) and beam-waist size ($w_o = 100\ \mu$m); the considered phase-

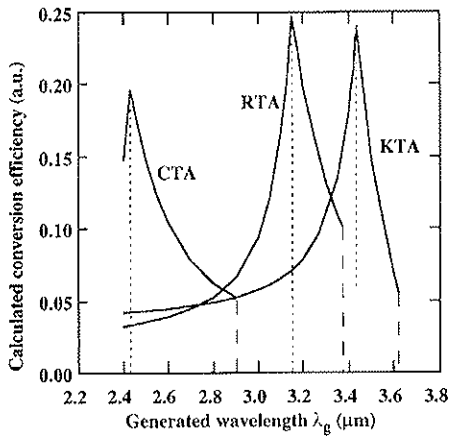

Fig. 7. Calculated conversion efficiency for type I DFG along the phase-matching direction of maximum nonlinear effective coefficient, as a function of the generated wavelength λ_g. Crystal length $L = 10$ mm, beam-waist radius $w_o = 100\ \mu$m, $\lambda_p = 1.064\ \mu$m. The refractive indices are calculated from Eq. (3) and Table 1, and the nonlinear coefficients are taken from Ref. 9.

matching direction is the one associated with the maximum nonlinear effective coefficient. For increasing λ_g, this direction, which is located in the $x-z$ plane, comes nearer to the x axis, as shown in Fig. 3(a), and then passes in the $x-y$ plane. The walk-off angle ρ then decreases with increasing λ_g, with minimum values ($\rho = 0$) along the x and y axes. At the same time, the associated nonlinear effective coefficient decreases for direction nearer to the y axis, because $\chi_{15} < \chi_{24}$ for these compounds. The calculated conversion efficiency then exhibits a maximum for the wavelength generated along the x axis, which is different for each of the three crystals. Depending on the desired wavelength and on the focusing conditions, the best arsenate isomorph may be chosen for this particular situation.

REFERENCES

1. P. E. Powers, S. Ramakrishna, C. L. Tang, and L. K. Cheng, "Optical parametric oscillation with $KTiOAsO_4$," Opt. Lett. **18**, 1171–1173 (1993).
2. P. E. Powers, C. L. Tang, and L. K. Cheng, "High-repetition-rate femtosecond optical parametric oscillator based on $RbTiOAsO_4$," Opt. Lett. **19**, 1439–1441 (1994).
3. D. T. Reid, M. Ebrahimzadeh, and W. Sibbett, "Ti:sapphire-pumped femtosecond optical parametric oscillator based on $KTiOPO_4$ and $RbTiOAsO_4$," Appl. Phys. B: Lasers Opt. **60**, 437–442 (1995).
4. P. E. Powers, C. L. Tang, and L. K. Cheng, "High-repetition-rate femtosecond optical parametric oscillator based on $CsTiOAsO_4$," Opt. Lett. **19**, 37–39 (1994).
5. W. R. Bosenberg, L. K. Cheng, and J. D. Bierlein, "Optical parametric frequency conversion properties of $KTiOAsO_4$," *Conference on Lasers and Electro-Optics*, Vol. 11 of 1993 OSA Technical Digest Series (Optical Society of America, Washington, D.C. 1993), pp. 430–432.
6. D. L. Fenimore, K. L. Schepler, D. Zelmon, S. Kück, U. B. Ramabadran, P. Von Richter, and D. Small, "Rubidium titanyl arsenate difference-frequency generation and validation of new Sellmeier coefficients," J. Opt. Soc. Am. B **13**, 1935–1940 (1996).
7. D. L. Fenimore, K. L. Schepler, U. B. Ramabadran, and S. R. MacPherson, "Infrared corrected Sellmeier coefficients for potassium titanyl arsenate," J. Opt. Soc. Am. B **12**, 794–796 (1995).
8. G. T. Kennedy, D. T. Reid, A. Miller, M. Ebrahimzadeh, H. Karlsson, G. Arivdsson, and F. Laurell, "Near- to mid-infrared picosecond optical parametric oscillator based on periodically poled $RbTiOAsO_4$," Opt. Lett. **23**, 503–505 (1998).
9. B. Boulanger, J. P. Fève, B. Ménaert, and G. Marnier, "Methodology for optical studies of nonlinear crystals: application to the isomorph family $KTiOPO_4$, $KTiOAsO_4$, $RbTiOAsO_4$, and $CsTiOAsO_4$," Pure Appl. Opt. **7**, 239–256 (1998).
10. I. Rousseau, B. Boulanger, J. P. Fève, and O. Pacaud, "Extended sphere method for complete investigation of the phase-matching properties sum- and difference-frequency generation," Appl. Opt. **38**, 7406–7408 (1999).
11. G. Marnier, "Process for the flux synthesis of crystals of the $KTiOPO_4$, potassium titanyl monophosphate type," French patent FR 2585345 (January 30, 1987); U.S. patent 4746396 (May 24, 1988).
12. G. M. Loiacono, D. N. Loiacono, and R. A. Stolzenberger, "Crystal growth and characterization of ferroelectric $CsTiOAsO_4$," J. Cryst. Growth **131**, 323–330 (1993).
13. B. Boulanger and G. Marnier, "Field factor calculation for the study of the relationships between all 3-wave nonlinear optical interactions in uniaxial and biaxial acentric crystals," J. Phys.: Condens. Matter **3**, 8327–8350 (1991).
14. D. A. Roberts, "Dispersion equations for nonlinear optical crystals: KDP, $AgGaSe_2$, and $AgGaS_2$," Appl. Opt. **35**, 4677–4688 (1996).
15. J. P. Fève, B. Boulanger, and G. Marnier, "Experimental study of internal and external conical refractions in KTP," Opt. Commun. **105**, 243–252 (1994).
16. L. T. Cheng, L. K. Cheng, and J. D. Bierlein, "Linear and nonlinear optical properties of the arsenate isomorphs of KTP," in *Growth, Characterization, and Applications of Laser Host and Nonlinear Crystals II*, B. H. Chai, ed., Proc. SPIE **1863**, 43–53 (1993).
17. G. E. Kugel, F. Bréhat, B. Wyncke, M. D. Fontana, G. Marnier, C. Carabatos-Nedelec, and J. Mangin, "The vibrational spectrum of a $KTiOPO_4$ single crystal studied by Raman and infrared reflectivity spectroscopy," J. Phys. C **21**, 5565–5583 (1988).
18. A. Khodjaoui, J. Mangin, and G. Marnier, "Dielectric properties of KTA and secondary optical absorption of KTA and KTP," Nonlinear Opt. **6**, 1–12 (1993).
19. B. Ruffing, A. Nebel, and R. Wallenstein, "All-solid-state cw mode-locked picosecond $KTiOAsO_4$ (KTA) optical parametric oscillator," Appl. Phys. B: Lasers Opt. **67**, 537–544 (1998).